A Statistical Variable Selection Solution for RFM Ill-Posedness and Overparameterization Problems

Sayyed Hamed Alizadeh Moghaddam, Mehdi Mokhtarzade, Amin Alizadeh Naeini, and AliReza Amiri-Simkooei

***Abstract*— Parameters of a rational function model (RFM), known as rational polynomial coefficients, are commonly redundant and highly correlated, leading to the problems of overparameterization and ill-posedness, respectively. In this paper, an innovative two-stage statistical method, called an uncorrelated and statistically significant RFM (USS-RFM), is presented to deal directly with these two problems. In the first stage, the proposed method employs a novel correlation analysis, which aims to exclude highly correlated coefficients. In the second stage, a new iterative significance test is applied to detect and remove unnecessary coefficients from the RFM. The proposed method is implemented on eight real data sets captured by Cartosat-1, GeoEye-1, Pleiades, Spot-3, and WorldView-3 platforms. The results are evaluated in terms of the positioning accuracy, model degrees of freedom, processing time, and figure condition analysis. Experimental results prove the efficiency of the proposed method, showing that it could achieve subpixel accuracy even for cases with five ground control points. The proposed USS-RFM is compared to an ℓ_1-norm regularization (L1R) technique and a particle swarm optimization (PSO) algorithm in the terrain-dependent case of the RFM. The results demonstrate the superiority of the USS-RFM, which performs better than the alternative methods in terms of positioning accuracy by more than 50% on average. Moreover, the RFMs resulted from the USS-RFM demonstrate to have higher degrees of freedom and, as a result, higher level of reliability. From the perspective of processing time, USS-RFM and L1R are similar while both are much faster than PSO.**

***Index Terms*— Ill-posedness, overparameterization, rational function model (RFM), statistical solution.**

I. Introduction

SATELLITE images are promising data sources for multifarious purposes, including thematic map production and digital elevation model (DEM) generation [1]. For extracting detailed and accurate geometric information from remotely sensed images, it is of prime importance to precisely define the mathematical relationship between image and ground spaces. To accomplish this, sensor models are employed [2].

Generally speaking, there are two types of sensor models, namely, rigorous and generic models [3]. Rigorous models thoroughly consider the geometry of the image at the time of the imagery [4]. Therefore, these models are sensor-dependent, which makes their application expensive, time-consuming, and prone to error [5]. They also require ancillary data, such as ephemeris, altitude, or other parameters of the satellite platform that are not always provided by the vendors [6]. All these disadvantages justify the application of generic models, which do not consider the geometry of the image at the time of imaging.

Among various generic models, none is more popular than the rational function model (RFM). The RFM has been exploited for various purposes, including digital surface model generation [7], rigorous sensor model recovery [8], 3-D reconstruction [9], [10], and bundle block adjustment [11]–[14], to name only a few. The RFM is classified into two cases in the literature. Strictly speaking, if the RFM employs rigorous models to estimate its own parameters, i.e., its rational polynomial coefficients (RPCs), it is known as a terrain-independent RFM. On the other hand, the RFM is highly terrain-dependent if its RPCs are estimated using ground control points (GCPs) [2].

The foremost criticism of the RFM, especially in the terrain-dependent case, is the presence of numerous RPCs, most of which are unnecessary and significantly correlated [5], [15]. This causes the problems of overparameterization and ill-posedness in the model. Although these problems are closely related, they are different in principle.

From the theoretical point of view, a problem is ill-posed, or equivalently ill-conditioned, when the outputs are sensitive to small changes in data [16]. This is the direct consequence of the multicollinearity of design or normal matrix that can be defined as the existence of nearly linear dependence among column vectors of these matrices [16].

The RFM, which is made up of four 3-D polynomials, contains a large number of correlated terms. In other words, the RFM suffers severely from the existence of numerous RPCs most of which are highly correlated. This causes the multicollinearity of the design and normal matrices in the

Manuscript received October 20, 2017; revised January 13, 2018 and February 22, 2018; accepted March 20, 2018. Date of publication April 17, 2018; date of current version June 22, 2018. *(Corresponding author: Sayyed Hamed Alizadeh Moghaddam.)*

S. H. Alizadeh Moghaddam and M. Mokhtarzade are with the Faculty of Geodesy and Geomatics Engineering, Khajeh Nasir Toosi University of Technology, Tehran 1996715433, Iran (e-mail: h.alizadeh@email.kntu.ac.ir; m_mokhtarzade@kntu.ac.ir).

A. Alizadeh Naeini and A. Amiri-Simkooei are with the Department of Geomatics Engineering, Faculty of Civil Engineering and Transportation, University of Isfahan, Isfahan 8174673441, Iran (e-mail: a.alizadeh@eng.ui.ac.ir; amiri@eng.ui.ac.ir).

Color versions of one or more of the figures in this paper are available online at http://ieeexplore.ieee.org.

Digital Object Identifier 10.1109/TGRS.2018.2819136

RFM's solution that means the RFM is very prone to the problem of ill-posedness.

The overparametrization, also called overfitting, is another problem in all interpolative models, including the RFM. It is defined as the "production of an analysis that corresponds too closely or exactly to a particular set of data and may, therefore, fail to fit additional data or predict future observations reliably" [17]. This problem occurs when the model contains more parameters than can be justified by the data [18]. In other words, the existence of unnecessary RPCs is the primary reason for the overparametrization problem, which causes the RFM to be burdened with errors.

Therefore, it is of prime importance to tackle these problems (i.e., overparametrization and ill-posedness) before applying RFM, especially in the case of terrain-dependent. Addressing these problems is our aim in this paper.

In the literature, two main categories of approaches to dealing with the problems of overparameterization and ill-posedness have been introduced: 1) variational regularization based on ℓ_0-norm [19], [20], ℓ_1-norm [5], [21], and ℓ_2-norm techniques [2] and 2) variable selection methods [22], [23].

The ℓ_2-norm, in contrast to the ℓ_0-norm and ℓ_1-norm techniques, does not exclude any RPCs from the RFM; therefore, it cannot address the overparameterization problem of the RFM. Rigorously, this regularization technique, also known as the Tikhonov method or ridge estimation in the literature, only attempts to make the RFM solution less ill-posed or even to make it well-posed, by adjusting the diagonal elements of the normal matrix. Consequently, the ℓ_2-norm regularization technique reduces the conditional number of the normal matrix and, as a result, yields an improvement in the stability of the RFM solution [4].

Long *et al.* [5] reported that the ℓ_0-norm regularization technique is computationally expensive. This is because this method employs a time-consuming search strategy to find a unique solution. These researchers also investigated the capabilities of the ℓ_1-norm regularization (L1R) technique. This technique, which is based on convex optimization algorithms, leads to a sparse vector of unknown RPCs with a few nonzero elements.

Forward selection and backward elimination [24] are two conventional variable selection methods that look for a suitable subset of the model's variables. Because a sequential search strategy is used in these two methods, the derived model may not necessarily be globally optimum [15]. Recently, some new variable selection methods have been proposed to select the optimal structure of the RFM based on the scatter matrix and elimination transformation [25], correlation analysis [26], nested regression [27], stepwise-then-orthogonal regression [28], and metaheuristic optimization algorithms [6], [15], [29].

In a major advance, Zoej *et al.* [6] employed a metaheuristic optimization algorithm to deal with the aforementioned problems by finding the optimal structure of the terrain-dependent RFM. These researchers applied a genetic algorithm (GA) to minimize the root-mean-square error (RMSE) computed over dependent check points (DCPs). In their method, control points (CPs) are divided into three groups as follows: 1) GCPs that are used to estimate the unknown RPCs; 2) DCPs that are used to calculate the objective function of the optimization algorithm; and 3) independent check points (ICPs) that are used to evaluate the quality of the ultimate RFM. This means that both GCPs and DCPs are required in this method, which considerably increases the need for CPs. Furthermore, metaheuristic optimization algorithms, such as GA or particle swarm optimization (PSO), have a high computational burden. Above all, their solutions may be unstable, since they may yield to different solutions in different runs [30].

The foregoing literature review implies that dealing with the RFM's problems has attracted considerable attentions, especially in the case of the terrain-dependent RFM. However, none of the reviewed methods can directly address the mentioned problems. In this paper, we propose a statistical two-stage method, namely, the uncorrelated and statistically significant RFM (USS-RFM), that belongs to the variable selection category. The USS-RFM, in fact, directly and effectively overcomes the problems of overparameterization and ill-posedness in the RFM by excluding the highly correlated and unnecessary RPCs, which are the main reasons for the mentioned problems.

The first stage of the USS-RFM is mainly designed to tackle the problem of ill-posedness by excluding highly correlated RPCs, while the second stage of the USS-RFM is applied as a complementary stage to the USS-RFM's first stage with the purpose of addressing the overparameterization issue. The second stage, in fact, detects and excludes the unnecessary RPCs from those obtained in the first stage. In our view, the proposed method is the first of its kind that directly and consistently addresses both problems of the RFM, namely, overparameterization and ill-posedness.

The proposed correlation analysis, in the first stage of the USS-RFM, can measure the correlation coefficients among RPCs prior to their estimation. However, in the conventional correlation analysis applied in [26] in the context of RFM, one has to estimate the RPCs in advance as a prerequisite for the correlation analysis. This imposes a restriction, that is, a large number of GCPs should exist for an accurate estimation of the RPCs [31]. In addition, the RPCs, which are estimated prior to the removal of highly correlated ones, are affected by the problem of ill-posedness. Therefore, they do not make a reliable basis for the correlation analysis used in [26].

The proposed USS-RFM does not have the mentioned disadvantages of the variable selection methods based on the metaheuristic optimization algorithms. It means that USS-RFM is appealing from the computational point of view and also providing a stable solution. In contrast to some of the exciting methods, such as [2], [6], [25], [26], [28], and [29], the USS-RFM has the outstanding characteristic that can be applied even with a limited number of GCPs, say five GCPs in our experiments.

Section II outlines the theoretical background of the RFM, the significance test, and the accuracy assessment measures. The methodology is described in Section III. In Section IV, the results of the experiments are provided, as well as some discussion. Our conclusions are drawn in Section V.

II. Theoretical Background

A. Rational Function Model

An RFM consists of mathematical equations attempting to model the spatial relationship between ground and image spaces. This model expresses the relationship in terms of the ratios of two third-order polynomial functions as follows [2]:

$$l = \frac{P_1(X,Y,Z)}{P_2(X,Y,Z)}, \quad s = \frac{P_3(X,Y,Z)}{P_4(X,Y,Z)} \tag{1}$$

$$P_1(X,Y,Z) = a_1 + a_2X + a_3Y + \cdots + a_{20}Z^3 \tag{2}$$

$$P_2(X,Y,Z) = 1 + a_{21}X + a_{22}Y + \cdots + a_{39}Z^3 \tag{3}$$

$$P_3(X,Y,Z) = b_1 + b_2X + b_3Y + \cdots + b_{20}Z^3 \tag{4}$$

$$P_4(X,Y,Z) = 1 + b_{21}X + b_{22}Y + \cdots + b_{39}Z^3 \tag{5}$$

where l and s are, respectively, the normalized line and sample coordinates of a point in the image space, and X, Y, and Z are their corresponding normalized coordinates in the ground space [5]. The terms a_i and b_i $(i = 1, 2, \ldots, 39)$ are the RFM's parameters, known as RPCs.

Although the RFM is a nonlinear model, it is usually expressed in a linear form via the following reformulation [5], [27]:

$$\begin{aligned} P_1(X,Y,Z) - lP_2(X,Y,Z) &= 0 \\ P_3(X,Y,Z) - sP_4(X,Y,Z) &= 0. \end{aligned} \tag{6}$$

For the purpose of estimating the RPCs, the standard linear Gauss–Markov model can be applied on (6) as follows:

$$\mathbf{y} = A\mathbf{x} + \mathbf{e} \tag{7}$$

where $\mathbf{y}$ is the vector of observations, A is the design matrix, $\mathbf{x}$ is the unknown parameters vector, and $\mathbf{e}$ is the vector of random errors [32]. $\mathbf{x}$ can be approximated using a least squares (LS) estimation, as $\hat{\mathbf{x}} = (A^\top PA)^{-1}A^\top P\mathbf{y}$, where P is the weight matrix of the observations. Applying (7), we can write the observation equations of r GCPs as follows:

$$A = \left[\begin{array}{c|c} A_l & \mathbf{0} \\ \hline \mathbf{0} & A_s \end{array}\right]_{2r\times 78} \tag{8}$$

$$A_l = [A_{l1}, A_{l2}, \ldots, A_{lr}]^\top \tag{9}$$

$$A_s = [A_{s1}, A_{s2}, \ldots, A_{sr}]^\top \tag{10}$$

$$A_{li} = \left[1, X_i, Y_i, \ldots, Z_i^3, -l_iX_i, -l_iY_i, \ldots, -l_iZ_i^3\right]^\top \tag{11}$$

$$A_{si} = \left[1, X_i, Y_i, \ldots, Z_i^3, -s_iX_i, -s_iY_i, \ldots, -s_iZ_i^3\right]^\top \tag{12}$$

$$\mathbf{y} = [l_1, l_2, \ldots, l_r, s_1, s_2, \ldots, s_r]^\top \tag{13}$$

$$\mathbf{x} = [a_1, a_2, \ldots, a_{39}, b_1, b_2, \ldots, b_{39}]^\top \tag{14}$$

where A_l and A_s are $r \times 39$ design matrices of lines and samples, respectively. Other symbols are the same as those in (1) and (7).

B. Significance Test

Models with numerous insignificant and unnecessary parameters have a low level of prediction because the problem of overparameterization leads to lower redundancy in the model. To reject parameters that do not contribute significantly to the model, the significance test can be employed [24]. Since insignificant parameters have values close to zero, the significance test can be written as follows [33]:

$$H_0 : \hat{x}_i = 0, \quad H_1 : \hat{x}_i \neq 0$$

$$S_i = \frac{\hat{x}_i}{\hat{\sigma}_{x_i}} \tag{15}$$

where $\hat{x}_i$ denotes the ith estimated parameter of the model, and S_i and $\hat{\sigma}_{x_i}$ are its corresponding test statistic and estimated standard deviation, respectively. The above-mentioned test statistic has a Student's t-distribution [33]. According to the LS estimation, $\hat{\sigma}_{x_i}$ is the square root of the ith diagonal elements in matrix $Q_{\mathbf{x}}$ that is calculated by applying the following equations:

$$\text{diag}(Q_{\mathbf{x}}) = \left[\hat{\sigma}_{x_1}^2, \hat{\sigma}_{x_2}^2, \ldots, \hat{\sigma}_{x_i}^2, \ldots, \hat{\sigma}_{x_p}^2\right] \tag{16}$$

$$Q_{\mathbf{x}} = \hat{\sigma}_0^2(A^\top PA)^{-1} \tag{17}$$

$$\hat{\sigma}_0^2 = \frac{\hat{\mathbf{e}}^\top P\hat{\mathbf{e}}}{df} \tag{18}$$

$$df = m - p \tag{19}$$

$$\hat{\mathbf{e}} = \mathbf{y} - A\hat{\mathbf{x}} \tag{20}$$

where A is the design matrix from (8)–(12), P is the weight matrix of observations, df represents the degrees of freedom, $\hat{\mathbf{e}}$ denotes the residual vector, $\hat{\sigma}_0^2$ is a variance factor, p and m are the total numbers of the estimated parameters and observations, respectively, $\hat{\mathbf{x}}$ is the vector of estimated parameters, and $Q_{\mathbf{x}}$ is its corresponding covariance matrix.

The aforementioned null hypothesis will be rejected if $|S_i| > t_{df,1-(\alpha/2)}$, where α is the significance level, $|.|$ denotes the absolute value operator, and t is the critical value extracted from the Student's t-distribution table with an upper cutoff value of $1 - (\alpha/2)$ and df as the degrees of freedom.

Rejection of the null hypothesis means that the estimated parameter is not statistically equal to zero. It is, therefore, a statistically significant parameter that must be preserved in the model. The parameters that fail to reject the null hypothesis are considered to be insignificant that can be excluded from the model.

C. Quality Assessment Measures

It is both common and necessary to evaluate the accuracy of a model estimated via GCPs. In the literature, three groups of quality or accuracy assessment measures have been introduced, each of which has its own merits. The first group indicates the goodness-of-fit of the estimated model. The RMSE and R-squared (21), which are both calculated over the GCPs, are good examples of this type of measure [27], [34]

$$R^2 = \frac{\sum_{i=1}^{m}(\hat{y}_i - \bar{y})^2}{\sum_{i=1}^{m}(y_i - \bar{y})^2}. \tag{21}$$

Equation (21) shows R-squared formula, in which $\bar{y}$ is the mean of observations, y_i denotes the ith observation value, $\hat{y}_i$ is the estimated value of the ith observation, and m denotes total number of observations. A high value of R^2 indicates that the model appropriately fits the GCPs. Note that R^2 has a value in the range [0, 1].

The second and the most widely used group of accuracy assessment measures is composed of measures calculated over ICPs. This group has the following disadvantages. First, the ICPs may not exist in mountainous or forested regions [35]. Second, it is expensive to provide CPs; therefore, it is not economical to reserve some ICPs from the CPs and leave the remaining as GCPs. This is important because a model estimated with more GCPs is more reliable. Finally, the misfit measures upon ICPs are pointwise, which means it is not possible to evaluate the accuracy for every pixel of the entire image [36]. The RMSE calculated over the ICPs belongs to this group.

The last group of accuracy assessment measures, which evaluates the precision for every pixel of an image, was introduced to mitigate the disadvantages mentioned above. This measure employs the propagation law and is known as a figure condition analysis [35], [36].

In order to conduct the figure condition analysis, (7) is first differentiated with respect to the unknown parameters $\mathbf{x}$ and the ground coordinates $\mathbf{l} = (X, Y, Z)$ [36]. This yields the following equations:

$$\delta \mathbf{y}_i = A_i \delta \mathbf{x} + B_i \delta \mathbf{l}_i \tag{22}$$

$$B_i = \begin{bmatrix} \dfrac{\partial l}{\partial X_i} & \dfrac{\partial l}{\partial Y_i} & \dfrac{\partial l}{\partial Z_i} \\ \dfrac{\partial s}{\partial X_i} & \dfrac{\partial s}{\partial Y_i} & \dfrac{\partial s}{\partial Z_i} \end{bmatrix} \tag{23}$$

where A_i and B_i are, respectively, the design (8)–(12) and coefficient matrices of the ith ground point. A_i is a function of $\mathbf{l}_i = (X_i, Y_i, Z_i)$, whereas B_i is a function of both $\mathbf{l}_i$ and $\mathbf{x}$. Note that the ground coordinate of the ith point ($\mathbf{l}_i$) is typically obtained from a DEM.

Second, the square of the differential equation (22) is taken [36]. This results in the covariance matrix of the ith point in the image space ($Q_{\mathbf{y}_i}$)

$$Q_{\mathbf{y}_i} = A_i Q_{\mathbf{x}} A_i^{\top} + B_i Q_{\mathbf{l}_i} B_i^{\top} \tag{24}$$

$$Q_{\mathbf{l}_i} = \begin{bmatrix} \sigma_{X_i}^2 & 0 & 0 \\ 0 & \sigma_{Y_i}^2 & 0 \\ 0 & 0 & \sigma_{Z_i}^2 \end{bmatrix}^{-1} \tag{25}$$

where $Q_{\mathbf{x}}$ is the covariance matrix of the estimated parameters (17)–(20), and $Q_{\mathbf{l}_i}$ is the inverse of a matrix consisting of the ground coordinate accuracies of the ith point ($\sigma_{X_i}, \sigma_{Y_i}, \sigma_{Z_i}$).

Finally, to approximate the precision of the location (σ_i) for the ith point with (l_i, s_i) as its image coordinates, the following equation should be applied:

$$\sigma_i = \sqrt{\text{trace}(Q_{\mathbf{y}_i})} = \sqrt{\sigma_{l_i}^2 + \sigma_{s_i}^2} \tag{26}$$

where $\sigma_{l_i}^2$ and $\sigma_{s_i}^2$ are the diagonal elements of the matrix $Q_{\mathbf{y}_i}$, specifying the precision of the ith point in the directions of line and sample, respectively.

III. Methodology

The main concerns with respect to the RFM, especially in the terrain-dependent case, are the problems of overparameterization and ill-posedness. This section introduces a statistical two-stage method called the USS-RFM to directly address these concerns. The USS-RFM, in fact, optimally determines the structure of the RFM. The resulting RPCs are neither correlated nor insignificant in our method. As shown in Fig. 1, the first stage of the USS-RFM attempts to recognize and exclude highly correlated RPCs using a new correlation analysis, while in the second stage, it aims to exclude the insignificant, i.e., unnecessary, RPCs from those obtained in the first stage. In other words, the first stage of the proposed method is mainly responsible for addressing the problems of ill-posedness, while the second stage is a solution to the problem of overparameterization.

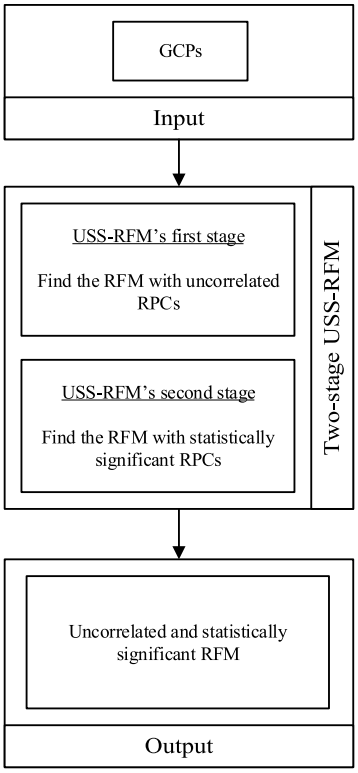

Fig. 1. Two-stage USS-RFM flow diagram.

A. USS-RFM: First Stage

In this section, our innovative correlation analysis is introduced. Subsequently, the proposed knowledge-based exclusion strategy (KES) is discussed. Finally, our procedure for recognizing and excluding highly correlated RPCs is explained step by step.

1) Correlation Analysis: To apply the correlation analysis, we propose a new method of computing correlation coefficients between every pair of RPCs. Pearson correlation [37] is adopted to measure the correlation coefficients between every pair of columns in the normal matrices ${A_l}^{\top} A_l$ and ${A_s}^{\top} A_s$, separately. This procedure yields two 39×39 symmetric correlation matrices, namely, $C_l = [\rho_{ij}^l]$ and $C_s = [\rho_{ij}^s]$, respectively, in which the component ρ_{ij} is the correlation coefficient between the ith and jth columns in the normal matrices. The degree of the linear dependence between the columns of the normal matrices can indicate the estability of their corresponding RPCs to be estimated. That is if two

columns of the normal matrix are nearly linearly dependent, their corresponding coefficients are highly correlated and hence can be poorly estimated. Employing the above-mentioned correlation analysis over the normal matrices has some advantages that will be described in the following.

For simplicity, we nominate hereafter the design matrix in the general form A, which can indicate either A_l (9) or A_s (10). For r distinct GCPs, we may partition the $r \times 39$ design matrix as $A = [\mathbf{g}_1, \mathbf{g}_1, \ldots, \mathbf{g}_{39}]$, where the r-vector $\mathbf{g}_i$ $(i = 1, \ldots, 39)$ is the ith column of A. We note that $\text{rank}(A) = \text{rank}(A^\top) = \text{rank}(A^\top A) = \min(r, 39)$, indicating that there exist at most 39 linearly independent columns (or rows) in the normal matrix $N = A^\top A$. However, when $r < 39$, only r coefficients at most can be identified by the correlation analysis. The correlation analysis can be implemented on the columns of A, the rows of $A^\top$, or the columns (or rows) of $A^\top A$.

This indicates that instead of computing $\text{corr}(\mathbf{g}_i, \mathbf{g}_j)$ on the columns of the design matrix A, we may use the normal matrix $N = A^\top A = [A^\top \mathbf{g}_1, A^\top \mathbf{g}_1, \ldots, A^\top \mathbf{g}_{39}]$, and hence compute $\text{corr}(A^\top \mathbf{g}_i, A^\top \mathbf{g}_j) = \text{corr}(n_i, n_j)$. This has advantages over the correlation analysis of the design matrix because, for $r < 39$, it transforms $\mathbf{g}_i \in R(A) = \mathbb{R}^r$ into a higher dimension vector $n_i = A^\top \mathbf{g}_i$, which belongs to $R(A^\top) = R(A^\top A) \subset \mathbb{R}^{39}$, where R is the range space of a matrix. A higher dimension vector is preferred because its corresponding correlation coefficient is calculated based on a larger number of samples, leading to more precise correlation coefficients. Furthermore, this strategy is conceptually similar to converting the identity metric tensor $(W = I)$ when computing the correlation coefficients. Our observations also show that such correlation coefficients are more stable than the classical ones. Further information on the above concepts can be found in [38] and [39].

The correlation matrices C_l and C_s are later used to detect and exclude highly correlated RPCs.

2) Knowledge-Based Exclusion Strategy: To exclude one of the two RPCs, recognized as a pair of highly correlated RPCs through the correlation analysis, we put forward an innovative KES. Suppose that a pair of RPCs, for instance, a_i and a_j $(i > j)$ are recognized to be highly correlated with each other. In order to discard one of these RPCs, KES excludes the coefficient with the higher index number. Therefore, here, a_i is excluded from the RFM.

In KES, as a result, there is a tendency to remove high-order terms in favor of low-order terms. Note that denominator terms, which are indexed by higher numbers [see (1)–(5)], are more prone to be omitted. The underlying reason for the design of such an exclusion strategy is that numerator and low-order polynomial terms (e.g., 3-D affine or DLT) have been found to be the appropriate terms for the RFM [40]–[43].

3) Steps of the USS-RFM First Stage: In this stage, as previously mentioned, the proposed method pursues the objective of recognizing and excluding highly correlated RPCs prior to RFM solution. Fig. 2 shows the diagram illustrating this stage.

The USS-RFM's first stage can be summarized by the following steps.

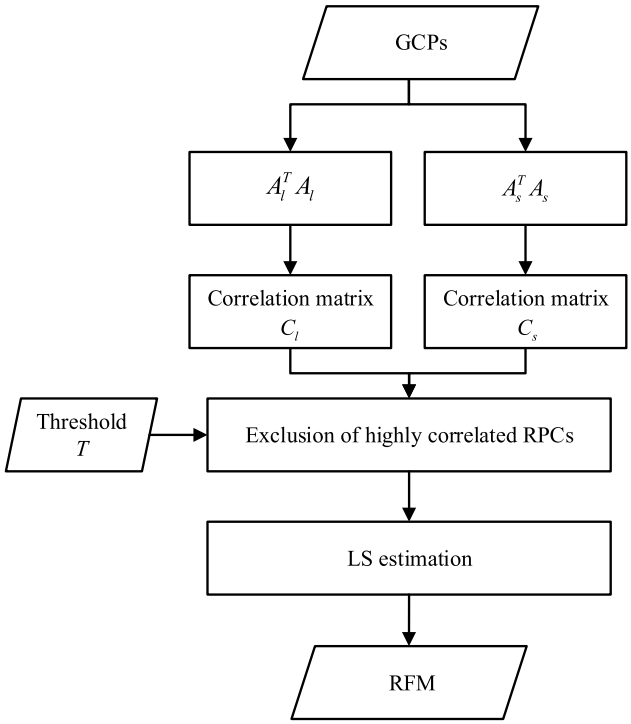

Fig. 2. Diagram of the USS-RFM's first stage.

Step 1: Compute the normal matrices ${A_l}^\top A_l$ and ${A_s}^\top A_s$ as described in (9) and (10).

Step 2: Calculate correlation matrices C_l and C_s by applying the above-mentioned correlation analysis (see Section III-A1)

Step 3: For C_l and C_s, separately, find the elements that $|\rho_{ij}| > T$. Each of the identified ρ_{ij} is associated with a pair of RPCs (i.e., the i-th and j-th RPCs) that is assumed to be highly correlated. Subsequently, employ the KES (see Section III-A2) to exclude one of the two highly correlated RPC in each pair.

Step 4: Employ LS estimation to solve the RFM with its remaining coefficients.

Threshold T in the above steps should be the one that yields the best performance of the ultimate RFM. R-squared is one of the most common criteria to measure the goodness-of-fit of the RFM. Therefore, at first glance, it seems that an optimum T should maximize the R-squared. However, in case R-squared is computed over GCPs, the model tends to have more numbers of RPCs in favor of better fit to GCPs, which intensifies the overparametrization problem.

To tackle this issue and to set the threshold T automatically, we propose the optimum value of T as the one that maximizes the following function:

$$f(T) = R^2(T) + \gamma \frac{df(T)}{2r} \tag{27}$$

where $R^2(T)$ and $df(T)$ are the R-squared (21) value and the degrees of freedom, respectively, for the estimated model associated with T, r denotes the total number of the GCPs, and γ is a constant value that balances the effects of both R^2 and df, normalized by $2r$, in the function $f(T)$.

In our experiments, we varied the value of T from 0.5 to 0.9. For every threshold value, steps 3 and 4 are repeated.

Then, the optimum value of T is the one which maximizes the function (27).

The first term of (27), as mentioned above, considers the goodness-of-fit of the ultimate model. The second term, however, is in charge to prevent the problem of overparameterization, which is interpreted continuously.

To manage the problem of overparameterization, an attempt should be made to keep the ratio of (p/m) as small as possible, where p and $m = 2r$ are the total numbers of remaining RPCs and observation equations, respectively. The smaller value of $[p/(2r)]$ is synonymous with the larger value of the second term in (27), i.e., $(df)/(2r) = 1 - (p/(2r))$. Since both terms of (27) are bounded in the range [0, 1], they can be integrated into one equation, while the constant γ manages the impact of each one. Based on our experiments, a small value of γ, say in the range $[10^{-7}, 10^{-5}]$, makes a good balance.

Regarding our algorithm, it should be noted that this always considers the zero-order coefficients a_1 and b_1 from both geometrical and mathematical point of view. From the geometrical perspective, these two coefficients must be preserved because they play the role of shift parameters, which is essential in the transformation from the ground space to the image space. In addition, as will be discussed later, the zero-order coefficients are not correlated with the other coefficients. Consequently, they do not cause the problem of ill-posedness from the mathematical perspective, and they can be preserved in the model.

Concerning the zero-order coefficients a_1 and b_1, the first column of A is a constant vector $\mathbf{g}_1 = \mathbf{c}$. The variance of the constant vector is zero by definition, i.e., $\text{var}(\mathbf{c}) = 0$. The covariance between the constant vector $\mathbf{c}$ and other columns $\mathbf{g}_i$ of A is also zero, i.e., $\text{cov}(\mathbf{c}, \mathbf{g}_i) = 0$. Taken together, these observations could indicate that the correlation $\text{corr}(\mathbf{g}_1 = \mathbf{c}, \mathbf{g}_i)$ is undefined because $(0/0)$ is not a number (NaN). This is, however, not the case because this issue is similar to the "limit" concept in mathematics. To see this, let us consider a small purely random noise ϵ added to the constant vector, i.e., $\mathbf{c} + \epsilon$. We then have $\text{var}(\mathbf{c} + \epsilon) = \sigma_\epsilon$, and $\text{cov}(\mathbf{c} + \epsilon, \mathbf{g}_i) = \text{cov}(\mathbf{c}, \mathbf{g}_i) + \text{cov}(\epsilon, \mathbf{g}_i) = 0$, resulting in $\text{corr}(\mathbf{c} + \epsilon, \mathbf{g}_i) = 0$. When considering the correlations in the normal matrix, one can argue by a similar reasoning that the computed correlations of the zero-order coefficients make no sense. We, therefore, assume that the zero-order coefficients a_1 and b_1 do not correlate with the other coefficients. This statement has also been verified using simulated data sets.

B. USS-RFM: Second Stage

In the second stage of the USS-RFM, a recursive significance test is proposed to ensure that no insignificant and unnecessary RPCs exist in the RFM. Fig. 3 shows the flow diagram of the second stage.

The USS-RFM's second stage is composed of the following steps.

Step 1: Conduct the significance test (15)–(20) on the current RFM.

Step 2: Recognize the insignificant RPCs and exclude them from the RFM.

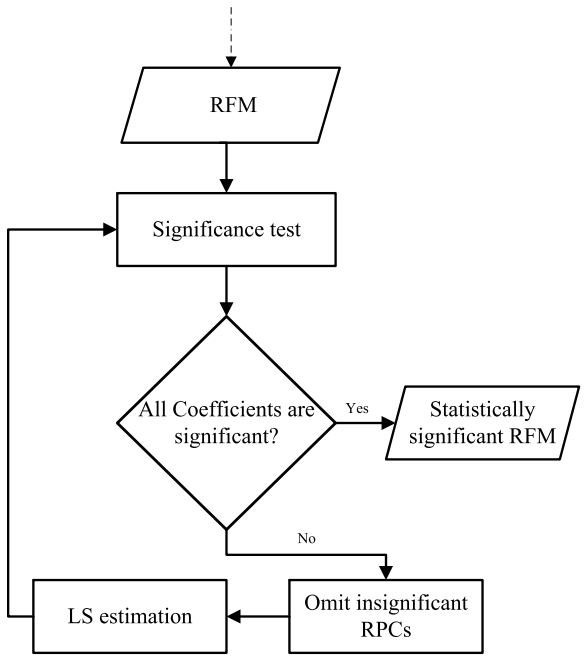

Fig. 3. Flow diagram of the USS-RFM's second stage.

TABLE I
DATA SET SPECIFICATIONS

Data set	Platform	Area type	Level of correction	Off nadir angle (deg)	GSD (m)	Elevation range (m)	NO. CPs
Geo-ISF	GeoEye-1	Urban	Primary	15.7	0.5	15	50
Geo-UR	GeoEye-1	Urban	Primary	0.8	0.5	185	50
PL-ISF	Pleiades	Urban	Primary	8.4	0.5	10	50
WV-ISF	WorldView-3	Urban	Primary	1.4	0.5	8	50
C1-KS	Cartosat-1	Rural, Mountainous	Primary	5	2.5	570	80
C1-TH	Cartosat-1	Semi-urban	Primary	5	2.5	150	26
S1A-ISF	Spot-3 1A	Rural, Mountainous	Raw	19	10	613	28
S1B-ISF	Spot-3 1B	Rural, Mountainous	Primary	19	10	613	28

Step 3: Reestimate the RFM with the remaining RPCs.

Step 4: Repeat steps 1 to 3 until no insignificant RPCs exist.

As mentioned in Section II-B, the significance test, similar to other statistical tests, needs a parameter, namely, significance level (α) to be set by the user. Because we employed this test in the second stage of the proposed method, α is considered as a parameter of the proposed USS-RFM that must be valued.

IV. EXPERIMENTS

A. Data Sets

In our experiments, eight real data sets were used (see Table I). The CPs for the two Spot-3 data sets were measured applying a differential GPS technique, which is accurate for better than 1 m. CPs for the other case studies were collected from 1:2000 digital reference maps. The accuracy of these points, which were chosen from distinct image/map features, is assumed to be better than 1 m. Table I provides more information about the data sets, which were all acquired from the different cities in the country of Iran.

According to Table I, the data sets cover a variety of image conditions that allow verifying the impacts of the input data characteristics on the performance of the proposed method. Our data sets contain different off-nadir angles

(ranging from 0.8° to 19°), ground sampling distances (GSDs) (ranging from 0.5 to 10 m), elevation ranges (ranging from 8 m in WV-ISF to 613 m in S1A-ISF), and different levels of geometric correction (e.g., S1A-ISF and S1B-ISF images were captured from the same area with different levels of geometric correction, namely, Level 1A and Level 1B, respectively).

In our experiments, we applied four very high spatial resolution (VHSR) images, i.e., Geo-UR, Geo-ISF, PL-ISF, and WV-ISF data sets with a GSD of 0.5 m, among which Geo-UR case study was collected over the city of Urmia, North West of Iran, while the other ones were acquired over different areas of the downtown Isfahan, Iran. These VHSR images were geometrically corrected at the primary level, including the corrections of Earth rotation and curvature, mirror look angles, and orbit characteristics.

We also applied two high spatial resolution images, namely, C1-KS and C1-TH, captured via Cartosat-1 platform. These two images are provided at the primary level of geometric correction. In addition, we applied two medium spatial resolution satellite images of Spot-3 (i.e., GSD $=$ 10 m) platform from the province of Isfahan, Iran. S1A-ISF was a geometrically raw image that has been undergone only a radiometric correction; however, the S1B-ISF data set was also corrected for the primary geometric distortions.

Beside each satellite image, an ASTER global DEM of the covering area with a horizontal accuracy of 1 arcsecond and a reported vertical accuracy of 12.62 m [44] was used for the figure condition analyses.

B. Competing Methods

The proposed method, which is suited for the terrain-dependent RFM, has the prominent characteristics of: 1) it can deal the problems of ill-posedness and overparametrization in the RFM's solution and 2) it has the outstanding characteristic that is applicable even with a small number of GCPs (e.g., five GCPs).

According to the above points, only the recent or common methods are qualified as the competing ones, which are concerned to manage the overparametrization and ill-posedness problems and can work with a small number of GCPs. From these aspects, L1R technique [5], PSO-based variable selection [29], and Tikhonov regularization technique [2] were selected as the competing methods.

The L1R and PSO methods are also very appealing because they both can work with a limited number of GCPs, and also they come from different categories dealing with the problems of ill-posedness and overparameterization (L1R is a regularization-based technique, but PSO is a variable selection method). In addition, Tikhonov regularization technique is very common in practice [5] and is directly concerned with the ill-posedness issue.

L1R should be solved through a convex optimization algorithm. For this purpose, the free package SpaSM was applied [45]. This package, which was also applied in [5], is based on the least absolute shrinkage and selection operator (Lasso) [46] via the least angle regression algorithm [21], [45], [47].

TABLE II
PSO PARAMETER SETTING

Parameter	Value
Population size	30
V_{max}	3
V_{min}	-3
w_{max}	1
w_{min}	0.02
t	200
C_1	1.5
C_2	1.5

C. Parameter Setting

The USS-RFM has two parameters, namely, γ and the significance level (α). In accordance with the RFM literature [5], γ was set manually. Experientially, 10^{-6} was the best value for all the remotely sensed data sets in this paper. The significance level α was set to 0.2 for the following reason. In the statistics literature, typical values for α range from 0.01 to 0.2 [48]–[50]. This value should be chosen and adjusted according to the application in hand. In our case, α, which is known as Type I error in the statistical literature, represents the probability of preserving an insignificant parameter. In contrast, Type II error, which is inversely related to α, indicates the probability of omitting a significant parameter by mistake. The elimination of necessary, i.e., significant parameters from the model can trap the model into difficulties. However, preserving a few unnecessary parameters does not seriously affect the model performance. We, therefore, took the Type I error (α) as 0.2 in our experiments.

Regarding the parameters of the competing methods, the PSO algorithm's parameters, set according to [29], are shown in Table II. The parameter for L1R, known as the regularization parameter, is a problem-dependent one that should be set by the user. In our experiments, this parameter is set optimally via a trial and error approach in every case study.

D. Results and Discussion

This section has been divided into four main parts. In the first two parts, the proposed method is compared with the traditional (i.e., Tikhonov and OLS) and recent (i.e., L1R and PSO) methods separately, from the perspectives of accuracy, processing time, and reliability. In the third part, the efficacy of the USS-RFM's second stage is discussed. In the last part, a continuous accuracy analysis, namely, the figure condition analysis is conducted on the RFMs derived from the proposed method.

1) Comparison to the Traditional Methods: The objective of this section is to verify the presence of the ill-posedness and overparameterization problems in the RFM with 78 RPCs and to show that the proposed USS-RFM can properly address these problems.

To accomplish this, the RFM was solved by applying two traditional methods, namely, ordinary least squares (OLS) and Tikhonov regularization technique [2]. Due to the existence of whole RPCs in these two methods (i.e., 78 RPCs), at least 39 well-distributed GCPs are required to solve the RFM.

TABLE III

RESULTS OBTAINED FROM TIKHONOV, OLS, AND THE PROPOSED USS-RFM

Data Set	RMSE of ICPs (pix)			Cond.		
	USS-RFM	Tikhonov	OLS	USS-RFM	Tikhonov	OLS
C1-KS	0.49	4.88	13.33	10.67	9.73E+10	1.52E+16
Geo-ISF	1.38	4.76	30.42	2.44	2.58E+11	1.14E+15
Geo-UR	0.56	2.59	2.46	1.29	1.11E+10	1.44E+16
PL-ISF	0.55	1.58	4.81	4.97	9.08E+10	6.29E+11
WV-ISF	0.58	3.98	4.27	8.32	1.20E+11	7.30E+11

Accordingly, C1-KS, Geo-ISF, Geo-UR, PL-ISF, and WV-ISF data sets, which have the minimum required GCPs, were selected from our case studies. In these data sets, 40 well-distributed GCPs were selected, and the remaining ones were served as the ICPs. The experimental results, i.e., RMSE calculated over the ICPs and the condition number of the normal matrix that is an index for ill-posedness problem [51] obtained from the USS-RFM, OLS, and Tikhonov methods are given in Table III. Note that, as recommended in [2], the regularization parameter of the Tikhonov method is set as $\lambda = 0.001$.

The large RMSEs and condition numbers of OLS verify that this method suffers considerably from the problem of ill-posedness and overparametrization. Although Tikhonov seems much better than OLS in the terms of condition numbers, it is not yet satisfying. One can, thus, conclude that Tikhonov only makes the RFM solution less ill-posed but not well-posed.

According to Table III, USS-RFM turns the RFM's ill-posed solution into a well-posed one, as it achieved considerably small condition numbers indicating the superiority of the proposed USS-RFM over the Tikhonov method. This is because in the USS-RFM, in contrast to the OLS and Tikhonov methods, some highly correlated and unnecessary RPCs are excluded from the RFM, which increase not only the degrees of freedom but also the interpretation and prediction capabilities of the model.

The satisfactory RMSE values and condition numbers resulted from the USS-RFM demonstrate that the proposed method addresses the problems of overparametrization and ill-posedness of the RFM effectively.

2) Comparison to the Recent Methods: In our experiments, the PSO algorithm was repeated 10 times and the best result was used for the comparison. As previously mentioned, the PSO algorithm requires some points to serve as DCPs. These points were selected from among the associated GCPs. In each experiment, different numbers of well-distributed GCPs were used, i.e., 5, 10, and 15 GCPs, whereas for PSO implementation two, five, and seven well-distributed DCPs were selected from among them. Table IV details the obtained results, with the best RMSE and df values shown in bold. A blank cell in this table means that the associated method could not find an acceptable RFM.

With regard to the accuracy, the USS-RFM outperforms the other methods in nearly all cases, which demonstrates the success of this method in addressing the problems of overparameterization and ill-posedness via removing highly correlated and insignificant RPCs. More importantly, the USS-RFM method can achieve subpixel accuracy even in the case of five GCPs. However, Table IV indicates the poor performance of the L1R method for the case of five GCPs, in line with findings in [5].

TABLE IV

OBTAINED RESULTS FROM THE PROPOSED USS-RFM, L1R TECHNIQUE, AND PSO ALGORITHM. df STANDS FOR THE DEGREES OF FREEDOM

Data Set	NO. GCPs\ICPs	RMSE of ICPs (pix)			*df*		
		USS-RFM	L1R	PSO	USS-RFM	L1R	PSO
C1-KS	5\75	**0.51**	-	-	**4**	-	-
	10\70	**0.48**	0.61	2.90	12	5	**15**
	15\65	**0.47**	0.48	0.66	**24**	13	23
C1-TH	5\21	**0.94**	-	7.21	**5**	-	4
	10\16	**0.88**	1.29	4.99	14	5	**15**
	15\11	**0.85**	1.35	1.24	**25**	9	23
Geo-ISF	5\45	**0.95**	-	3.40	**6**	-	4
	10\40	**0.94**	2.92	1.11	**16**	3	13
	15\35	0.98	1.39	**0.94**	**26**	11	24
Geo-UR	5\45	**0.64**	-	1.51	**7**	-	5
	10\40	0.61	1.66	**0.60**	**17**	1	16
	15\35	**0.59**	0.64	0.64	**27**	16	23
PL-ISF	5\45	**0.91**	-	-	**6**	-	-
	10\40	**0.85**	1.20	1.81	**14**	9	**14**
	15\35	**0.82**	0.97	1.15	**25**	16	23
S1A-ISF	5\23	9.54	-	**9.53**	**5**	**-**	**5**
	10\18	**0.74**	7.94	6.91	10	3	**13**
	15\13	**0.72**	0.88	3.83	18	3	**19**
S1B-ISF	5\23	**2.73**	-	-	**5**	-	-
	10\18	**0.98**	1.19	3.90	12	2	**13**
	15\13	**0.83**	1.12	1.12	21	7	**23**
WV-ISF	5\45	**0.88**	-	6.64	**6**	-	4
	10\40	**0.75**	1.40	1.20	**15**	5	**15**
	15\35	**0.72**	1.01	**0.72**	**25**	9	24

According to Table IV, none of the methods, including our proposed one, could achieve an acceptable RMSE for S1A-ISF data set in the case of applying five numbers of GCPs. A possible reason for this is that the S1A-ISF data set is geometrically a raw image. This indicates that the performance of the proposed method, similar to the competing methods, can be affected by the level of image's geometric correction. This lack of accuracy, however, can be addressed by applying more number of GCPs, as shown in Table IV.

As is apparent from Table I, we used various images with respect to off-nadir angle (ranging from 0.8° to 19°), GSD (ranging from 0.5 to 10 m), elevation range (ranging from 8 m in WV-ISF data set to 613 m in S1A-ISF data set), and the level of geometric correction. However, these levels of varieties could not trap the proposed method into difficulty because it achieved subpixel accuracy in almost all the cases with a small number of GCPs (see Table IV).

As seen in Table IV, the USS-RFM shows an average accuracy improvement of 53% over the L1R and 63% over PSO methods even when the cases with five GCPs are excluded. In addition, higher df values for the USS-RFM suggest a higher performance of the proposed method in terms of reliability. This is because, the reliability is directly related to the number of redundant observations, and hence to the degrees of the freedom [52]. The larger the number of observations is, the more the degrees of freedom is, and hence the more reliable the LS problem will be. The reliability concept can be generalized to any linear(ized) LS problem [39], [52].

From the computational aspect, the average processing times for USS-RFM, L1R, and 10 runs of the PSO algorithm

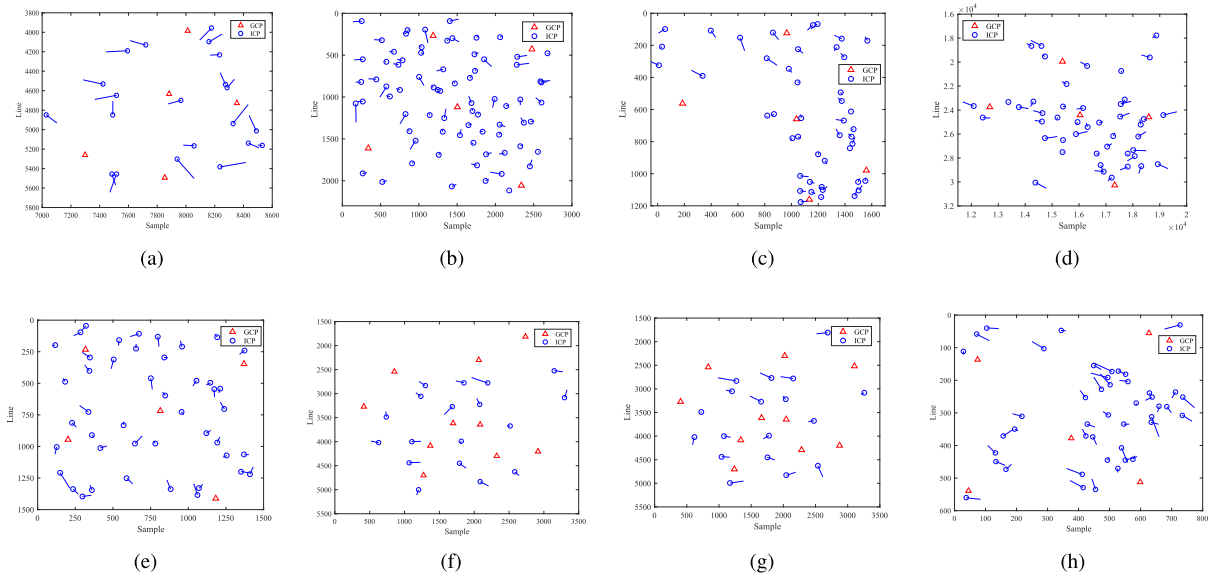

Fig. 4. CPs distribution together with the vectors of the residual error. (a) C1-TH. (b) C1-KS. (c) Geo-ISF. (d) Geo-UR. (e) PL-ISF. (f) S1A-ISF. (g) S1B-ISF. (h) WV-ISF.

were 0.08, 0.04, and 64 s, respectively. This leads to the conclusion that USS-RFM and L1R are similar with respect to runtime, while both are far faster than PSO.

Fig. 4 shows the CP distributions and ICPs' residual vectors for the case of subpixel accuracy and a minimum number of GCPs. A detailed look at Fig. 4 reveals no systematic behavior of the residual vectors. Note that for the sake of better illustration, the residual vectors have been scaled.

To verify the robustness of the proposed method against the GCPs' configuration, we repeated the experiments using different well-distributed configurations of GCPs. There was an acceptable consistency between the obtained results and those presented in Table IV.

3) Analyzing the Impact of USS-RFM's Second Stage: As previously mentioned, the USS-RFM consists of two stages: 1) the removal of highly correlated RPCs and 2) an iterative significance test on the remaining terms to detect and remove redundant RPCs. The second stage cannot be implemented alone for a limited number of GCPs. However, the first stage can be used in isolation as it removes the highly correlated terms prior to the RFM solution.

This section attempts to determine the impact of the USS-RFM's second stage when applied as a complementary process to the results obtained in the first stage. Table V compares the results of the USS-RFM's first stage (USS-RFM-1st) with those of the two-stage USS-RFM method.

At first glance, it may seem that the second stage only improves the performance from the reliability point of view (i.e., it increases the df in all cases). However, the advantage of the second stage on the positional accuracy is not clear. To reveal this aspect, we applied a Mann–Whitney U test [53], which is a common statistical test that can be applied to compare two independent set of samples. In our case, Mann–Whitney U test was used to determine if there is any statistically significant difference between the RMSE values resulted from the first stage of USS-RFM (USS-RFM-1st) and those from the two-stage USS-RFM.

TABLE V

RESULTS OBTAINED FROM THE USS-RFM'S FIRST STAGE (USS-RFM-1st) AND THE TWO-STAGE USS-RFM. df STANDS FOR THE DEGREES OF FREEDOM

Data Set	NO. GCPs\ICPs	RMSE of ICPs (pix)		df	
		USS-RFM-1st	USS-RFM	USS-RFM-1st	USS-RFM
C1-KS	5\75	0.52	0.51	2	4
	10\70	0.47	0.48	11	12
	15\65	0.47	0.47	22	24
C1-TH	5\21	1.43	0.94	1	5
	10\16	4.53	0.88	1	14
	15\11	0.99	0.85	18	25
Geo-ISF	5\45	2.50	0.95	1	6
	10\40	0.97	0.94	13	16
	15\35	1.00	0.98	24	26
Geo-UR	5\45	0.77	0.64	2	7
	10\40	0.64	0.61	13	17
	15\35	0.63	0.59	23	27
PL-ISF	5\45	1.01	0.91	3	6
	10\40	0.88	0.85	11	14
	15\35	0.91	0.82	20	25
S1A-ISF	5\23	7.95	9.54	1	5
	10\18	0.74	0.74	10	10
	15\13	0.70	0.72	16	18
S1B-ISF	5\23	3.75	2.73	1	5
	10\18	0.93	0.98	10	12
	15\13	0.89	0.83	15	21
WV-ISF	5\45	0.95	0.88	2	6
	10\40	0.84	0.75	8	15
	15\35	0.72	0.72	12	25

The general underlying concept of Mann–Whitney U test goes as follows. It combines the samples, coming from different sets, and then sorts them according to their value in the form of a queue. Sample sets are regarded to be statistically different if it is possible to consider them as two distinct clusters at the opposite ends of that queue. On the other hand, if the samples are randomly mixed, from the statistics point of view, the test will decide that their original sets are the same [53]. Mann–Whitney U test also has an attractive advantage that has no assumption about the statistical distribution of the sets.

The numbers of CPs were changed from 5 to 20 to make a sufficiently large statistical population. As a result,

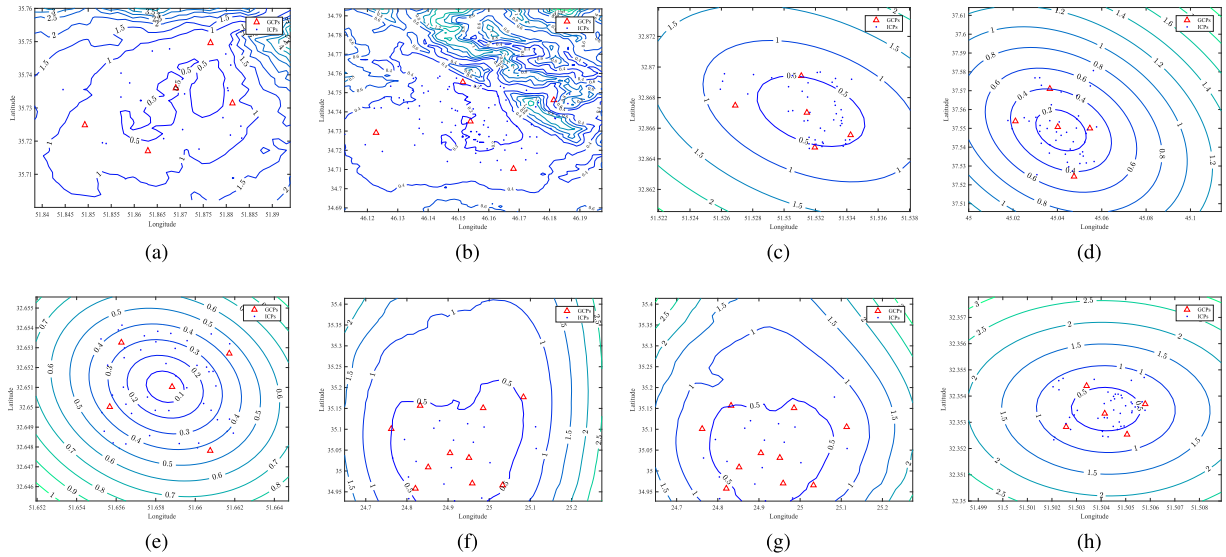

Fig. 5. Figure condition analysis. (a) C1-TH. (b) C1-KS. (c) Geo-ISF. (d) Geo-UR. (e) PL-ISF. (f) S1A-ISF. (g) S1B-ISF. (h) WV-ISF. For all data sets, except (f) and (g), five GCPs were applied. The unit of the contours is given in pixel.

16 RMSE values were generated for each data set, yielding 128 values for each case (i.e., USS-RFM-1st and the complete two-stage method). Subsequently, the Mann–Whitney U test was implemented using SPSS software. The obtained result proved that the improvement resulting from the USS-RFM's second stage is statistically significant at the 95% confidence level. Because the mean of RMSE values resulted from the USS-RFM is smaller than that of the USS-RFM-1st, we can conclude that the USS-RFM statistically outperforms USS-RFM-1st in the terms of positional accuracy. In other words, the second stage of the proposed method can statistically improve the positional accuracy if it is applied after the USS-RFM's first stage.

In addition to the improvements in the positional accuracy and reliability, the second stage of USS-RFM decreases the complexity of the model by excluding the unnecessary RPCs, remained from the first stage. This, as a result, improves the interpretation and prediction capabilities of the model [24].

4) Precision Analysis of the Proposed Method Using Figure Condition Analysis: Applying a figure condition analysis (22)–(26), we can achieve an accuracy analysis for every pixel of an image. In contrast to other accuracy measures, such as the RMSE of ICPs, the figure condition measure provides the user with a continuous accuracy analysis even for areas far from the CPs coverage. In view of the advantages of this accuracy measure, we conducted the figure condition analysis on the RFM derived from the USS-RFM method (see Fig. 5).

According to Fig. 5, and as previously shown in [35] and [36], the best figure condition results are obtained around the GCPs' coverage centroid. The RFM performance deteriorates with distance from the centroid. However, the performance degradation of the resultant RFM is very gentle and does not exceed three pixels even at the farthest corners. Therefore, it can be concluded that the USS-RFM performs well even for extrapolation purposes.

V. Conclusion

A large number of unnecessary RPCs, together with the significant correlations among them, are two primary factors that cause the degrading problems of overparameterization and ill-posedness in RFMs. To address these problems, we proposed an innovative statistical two-stage method called the USS-RFM. The underlying idea behind the proposed method was the integration of the correlation analysis and the significance test to remove redundant and highly correlated RPCs.

We applied various images in our experiments with different off-nadir angles, GSD terrain reliefs, and the levels of geometric correction (see Table I). However, we can conclude the robustness of the USS-RFM against the mentioned factors from Table IV because the USS-RFM achieved satisfying subpixel accuracy in almost all the cases.

The proposed method was compared with two state-of-the-art approaches, namely, L1R and PSO from the RFM literature. Regarding the comparison between the proposed method and its competitors, the USS-RFM appeared to provide the best performance, while being less demanding than PSO in terms of computation. According to the implementation results, the USS-RFM outperformed both PSO and L1R by more than 50% in the positioning accuracy, on average. It also proved to be applicable in cases where only a few GCPs exist, as shown by the results with only five GCPs. As a result, the proposed USS-RFM can be considered as a valuable method in the terrain-dependent case of the RFM.

As with any new research, there are some unresolved issues that may present challenges over time. In our view, one of the most important of these is an automatic selection of the γ parameter, which balances the impact of R^2 and the normalized df in the first stage of the proposed method. This parameter is currently selected manually. Methods for determining its value automatically could be a topic for future research.

ACKNOWLEDGMENT

The authors would like to thank Prof. M. J. V. Zoej from the K. N. Toosi University of technology, Tehran, Iran, Dr. S. Homayouni from the University of Ottawa, Ottawa, ON, Canada, and Dr. S. B. Fatemi from the University of Isfahan, Isfahan, Iran, for providing us with some data sets in our case studies. They would like to thank Dr. T. Long from the Chinese Academy of Sciences, Beijing, China, for his help in the implementation of L1R technique. They would also like to thank the anonymous reviewers who helped them to improve this paper.

REFERENCES

[1] M. Mokhtarzade and M. J. V. Zoej, "Road detection from high-resolution satellite images using artificial neural networks," *Int. J. Appl. Earth Observ. Geoinf.*, vol. 9, no. 1, pp. 32–40, 2007.

[2] C. V. Tao and Y. Hu, "A comprehensive study of the rational function model for photogrammetric processing," *Photogramm. Eng. Remote Sens.*, vol. 67, no. 12, pp. 1347–1358, 2001.

[3] T. Toutin, "Geometric processing of remote sensing images: Models, algorithms and methods," *Int. J. Remote Sens.*, vol. 25, no. 10, pp. 1893–1924, 2004.

[4] L. Zhang, X. He, T. Balz, X. Wei, and M. Liao, "Rational function modeling for spaceborne SAR datasets," *ISPRS J. Photogramm. Remote Sens.*, vol. 66, no. 1, pp. 133–145, 2011.

[5] T. Long, W. Jiao, and G. He, "RPC estimation via ℓ_1-norm-regularized least squares (L1LS)," *IEEE Trans. Geosci. Remote Sens.*, vol. 53, no. 8, pp. 4554–4567, Aug. 2015.

[6] M. J. V. Zoej, M. Mokhtarzade, A. Mansourian, H. Ebadi, and S. Sadeghian, "Rational function optimization using genetic algorithms," *Int. J. Appl. Earth Observ. Geoinf.*, vol. 9, no. 4, pp. 403–413, 2007.

[7] T. Toutin, "Radarsat-2 DSM Generation with new hybrid, deterministic, and empirical geometric modeling without GCP," *IEEE Trans. Geosci. Remote Sens.*, vol. 50, no. 5, pp. 2049–2055, May 2012.

[8] W.-C. Huang, G. Zhang, and D. Li, "Robust approach for recovery of rigorous sensor model using rational function model," *IEEE Trans. Geosci. Remote Sens.*, vol. 54, no. 7, pp. 4355–4361, Jul. 2016.

[9] Y. Gu, Z. Cao, and Y. Zhang, "Three-dimensional reconstruction of multiplatform stereo data with variance component estimation," *IEEE Trans. Geosci. Remote Sens.*, vol. 52, no. 7, pp. 4211–4226, Jul. 2014.

[10] G. Zhang, Z. Li, H.-B. Pan, Q. Qiang, and L. Zhai, "Orientation of spaceborne SAR stereo pairs employing the RPC adjustment model," *IEEE Trans. Geosci. Remote Sens.*, vol. 49, no. 7, pp. 2782–2792, Jul. 2011.

[11] T. A. Teo, L. C. Chen, C. L. Liu, Y. C. Tung, and W. Y. Wu, "DEM-aided block adjustment for satellite images with weak convergence geometry," *IEEE Trans. Geosci. Remote Sens.*, vol. 48, no. 4, pp. 1907–1918, Apr. 2010.

[12] Z. Xiong and Y. Zhang, "Bundle adjustment with rational polynomial camera models based on generic method," *IEEE Trans. Geosci. Remote Sens.*, vol. 49, no. 1, pp. 190–202, Jan. 2011.

[13] G. Zhang *et al.*, "Block adjustment for satellite imagery based on the strip constraint," *IEEE Trans. Geosci. Remote Sens.*, vol. 53, no. 2, pp. 933–941, Feb. 2015.

[14] Y. Zhang, Y. Wan, X. Huang, and X. Ling, "DEM-assisted RFM block adjustment of pushbroom nadir viewing HRS imagery," *IEEE Trans. Geosci. Remote Sens.*, vol. 54, no. 2, pp. 1025–1034, Feb. 2016.

[15] A. A. Naeini, S. H. A. Moghaddam, S. M. J. Mirzadeh, S. Homayouni, and S. B. Fatemi, "Multiobjective genetic optimization of terrain-independent RFMS for VHSR satellite images," *IEEE Geosci. Remote Sens. Lett.*, vol. 14, no. 8, pp. 1368–1372, Aug. 2017.

[16] F. Öztürk and F. Akdeniz, "Ill-conditioning and multicollinearity," *Linear Algebra Appl.*, vol. 321, nos. 1–3, pp. 295–305, 2000.

[17] A. Stevenson, *Oxford Dictionary of English* (Oxford Dictionary of English). Oxford, U.K.: OUP, 2010.

[18] B. Everitt and A. Skrondal, *The Cambridge Dictionary of Sociology*, vol. 106. Cambridge, U.K.: Cambridge Univ. Press, 2002.

[19] E. J. Candès and T. Tao, "Decoding by linear programming," *IEEE Trans. Inf. Theory*, vol. 51, no. 12, pp. 4203–4215, Dec. 2005.

[20] M. Nikolova, "Description of the minimizers of least squares regularized with ℓ_0-norm. Uniqueness of the global minimizer," *SIAM J. Imag. Sci.*, vol. 6, no. 2, pp. 904–937, 2013.

[21] M. Schmidt, "Lease squares optimization with L_1-norm regularization," Univ. British Columbia, Vancouver, BC, Canada, Tech. Rep., 2005.

[22] N. R. Draper and H. Smith, *Applied Regression Analysis*. Hoboken, NJ, USA: Wiley, 2014.

[23] T. Poggio, V. Torre, and C. Koch, "Computational vision and regularization theory," *Nature*, vol. 317, no. 6035, pp. 314–319, 1985.

[24] C. M. Andersen and R. Bro, "Variable selection in regression—A tutorial," *J. Chemometrics*, vol. 24, nos. 11–12, pp. 728–737, 2010.

[25] Y. Zhang, Y. Lu, L. Wang, and X. Huang, "A new approach on optimization of the rational function model of high-resolution satellite imagery," *IEEE Trans. Geosci. Remote Sens.*, vol. 50, no. 7, pp. 2758–2764, Jul. 2012.

[26] H.-G. Sohn, C.-H. Park, and H.-U. Yu, "Application of rational function model to satellite images with the correlation analysis," *KSCE J. Civil Eng.*, vol. 7, no. 5, pp. 585–593, 2003.

[27] L. Tengfei, J. Weili, and H. Guojin, "Nested regression based optimal selection (NRBOS) of Rational Polynomial Coefficients," *Photogramm. Eng. Remote Sens.*, vol. 80, no. 3, pp. 261–269, 2014.

[28] C. Li, X. Liu, Y. Zhang, and Z. Zhang, "A stepwise-then-orthogonal regression (STOR) with quality control for optimizing the RFM of high-resolution satellite imagery," *Photogramm. Eng. Remote Sens.*, vol. 83, no. 9, pp. 611–620, 2017.

[29] S. Yavari, M. J. V. Zoej, A. Mohammadzadeh, and M. Mokhtarzade, "Particle swarm optimization of RFM for georeferencing of satellite images," *IEEE Geosci. Remote Sens. Lett.*, vol. 10, no. 1, pp. 135–139, Jan. 2013.

[30] T. Kurban, P. Civicioglu, R. Kurban, and E. Besdok, "Comparison of evolutionary and swarm based computational techniques for multilevel color image thresholding," *Appl. Soft Comput.*, vol. 23, pp. 128–143, Oct. 2014.

[31] Y. Hu, V. Tao, and A. Croitoru, "Understanding the rational function model: Methods and applications," *Int. Arch. Photogramm. Remote Sens.*, vol. 20, no. 6, pp. 1–6, 2004.

[32] A. Amiri-Simkooei, "Formulation of L_1 norm minimization in gauss-Markov models," *J. Surv. Eng.*, vol. 129, no. 1, pp. 37–43, 2003.

[33] D. C. Montgomery, E. A. Peck, and G. G. Vining, *Introduction to Linear Regression Analysis*. Hoboken, NJ, USA Wiley, 2012.

[34] A. C. Cameron and F. A. Windmeijer, "An R-squared measure of goodness of fit for some common nonlinear regression models," *J. Econ.*, vol. 77, no. 2, pp. 329–342, 1997.

[35] E. Sertel, S. H. Kutoglu, and S. Kaya, "Geometric correction accuracy of different satellite sensor images: Application of figure condition," *Int. J. Remote Sens.*, vol. 28, no. 20, pp. 4685–4692, 2007.

[36] H. Topan and H. S. Kutoglu, "Georeferencing accuracy assessment of high-resolution satellite images using figure condition method," *IEEE Trans. Geosci. Remote Sens.*, vol. 47, no. 4, pp. 1256–1261, Apr. 2009.

[37] J. L. Rodgers and W. A. Nicewander, "Thirteen ways to look at the correlation coefficient," *Amer. Statist.*, vol. 42, no. 1, pp. 59–66, 1988.

[38] G. Strang and K. Borre, *Linear Algebra, Geodesy, and GPS*. Philadelphia, PA, USA: SIAM, 1997.

[39] P. Teunissen, D. Simons, and C. Tiberius, "Probability and observation theory," Delft Inst. Earth Observ. Space Syst., Delft Univ. Technol., Delft, The Netherlands, 2005.

[40] F. Dadrass and A. Azizi, "The affine projection model as a tool for rapid geo-coding of IRS-P5 satellite imagery," *Int. Arch. Photogramm., Remote Sens. Spatial Inf. Sci.*, vol. 37, no. B4, pp. 1317–1322, 2008.

[41] I. Dowman and J. T. Dolloff, "An evaluation of rational functions for photogrammetric restitution," *Int. Arch. Photogramm. Remote Sens.*, vol. 33, pp. 254–266, Jul. 2000.

[42] C. Fraser, H. Hanley, and T. Yamakawa, "Sub-metre geopositioning with Ikonos GEO imagery," in *Proc. Joint ISPRS Workshop High Resolution Mapping Space*, 2001, pp. 19–21.

[43] G. Vozikis, J. Jansa, and C. Fraser, "Alternative sensor orientation models for high resolution satellite imagery," *Photogrammetrie, Fernerkundung, Geoinform.*, no. 12, pp. 179–186, 2003.

[44] S. Mukherjee, P. K. Joshi, S. Mukherjee, A. Ghosh, R. D. Garg, and A. Mukhopadhyay, "Evaluation of vertical accuracy of open source Digital Elevation Model (DEM)," *Int. J. Appl. Earth Observ. Geoinf.*, vol. 21, pp. 205–217, Apr. 2013.

[45] K. Sjöstrand, L. H. Clemmensen, R. Larsen, and B. Ersbøll, "A MATLAB toolbox for sparse statistical modeling," *J. Statist. Softw.* [Online] Available: http://www2.imm.dtu.dk/projects/spasm/references/spasm.pdf

[46] R. Tibshirani, "Regression shrinkage and selection via the lasso," *J. Roy. Statist. Soc. B (Methodol.)*, vol. 58, no. 1, pp. 267–288, 1996.

[47] B. Efron, T. Hastie, I. Johnstone, and R. Tibshirani, "Least angle regression," *Ann. Statist.*, vol. 32, no. 2, pp. 407–499, 2004.

[48] S. A. Bortone, *Estuarine Indicators*. Boca Raton, FL, USA: CRC Press, 2004.
[49] J. Cohen, H. Rothstein, and M. Borenstein, *Power and Precision*, vol. 1. New York, NY, USA: Taylor & Francis, 2001.
[50] K. E. Newcomer, H. P. Hatry, and J. S. Wholey, *Handbook of Practical Program Evaluation*. Hoboken, NJ, USA: Wiley, 2015.
[51] J. Bundschuh and M. C. S. A, *Introduction to the Numerical Modeling of Groundwater and Geothermal Systems: Fundamentals of Mass, Energy and Solute Transport in Poroelastic Rocks* (Multiphysics Modeling). Boca Raton, FL, USA: CRC Press, 2010.
[52] W. Baarda, *A Testing Procedure for Use in Geodetic Networks* (Publications on Geodesy), 2nd ed. Delft, The Netherlands: Netherlands Geodetic Commission, 1968.
[53] G. W. Corder and D. I. Foreman, *Nonparametric Statistics for Non-Statisticians: A Step-by-Step Approach*. Hoboken, NJ, USA: Wiley, 2011.

Sayyed Hamed Alizadeh Moghaddam was born in 1994. He received the B.S. degree in survey engineering from the University of Isfahan, Isfahan, Iran, in 2016. He is currently pursuing the M.Sc. degree in remote sensing with the Khajeh Nasir Toosi University of Technology, Tehran, Iran.

His research interests include the geometric processing of satellite images, hyperspectral remote sensing, dimensionality reduction, and computational intelligence.

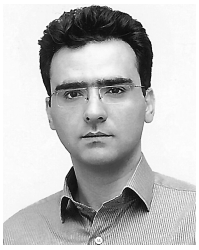

Mehdi Mokhtarzade received the M.Sc. and Ph.D. degrees in photogrammetry from the Khajeh Nasir Toosi University of Technology, Tehran, Iran, in 2004 and 2008, respectively.

He is currently an Associate Professor with the Khajeh Nasir Toosi University of Technology. His research interests include hyperspectral remote sensing, computational intelligence, georectification mathematical models, automatic feature extraction, and digital photogrammetry.

Amin Alizadeh Naeini received the B.S. degree in surveying and geomatics engineering from the University of Tabriz, Tabriz, Iran, in 2008, and the M.Sc. and Ph.D. degrees in photogrammetry from the University of Tehran, Tehran, Iran, in 2011 and 2015, respectively.

He has been an Assistant Professor with the Department of Geomatics Engineering, Faculty of Civil Engineering and Transportation, University of Isfahan, Isfahan, Iran, since 2015. His research interests include hyperspectral image processing, data fusion, pattern recognition, and the geometric processing of satellite images.

AliReza Amiri-Simkooei received the Ph.D. degree from the Mathematical Geodesy and Positioning Group, Faculty of Aerospace Engineering, Delft University of Technology, Delft, The Netherlands.

From 2007 to 2009, he was a Post-Doctoral Fellow with the Acoustic Remote Sensing Group, Delft University of Technology. Since 2009 and 2012, he has, respectively, been an Assistant and Associate Professor with the Department of Geomatics Engineering, Faculty of Civil Engineering and Transportation, University of Isfahan, Isfahan, Iran. He has authored over 50 research peer-reviewed journal papers in ISI journals. His research interests include the least-squares variance component estimation with applications to GPS data, advanced statistical estimation and approximation methods, precise positioning applications (land, water, and space) using space systems, assessment of noise characteristics and analysis of geoscience data series, and optimal design and subsequent analysis of geodetic control networks.

Dr. Amiri-Simkooei has been on the Editorial Board of the *Journal of Surveying Engineering*, ASCE, since 2010. He is currently an Associate Editor of the *Journal of Surveying Engineering*, ASCE.